Geometric Mechanics of Periodic Pleated Origami

Z. Y. Wei,[1] Z. V. Guo,[1] L. Dudte,[1] H. Y. Liang,[1] and L. Mahadevan[1,2,*]

[1]School of Engineering and Applied Sciences, Harvard University, Cambridge, Massachusetts 02138, USA
[2]Department of Physics, Harvard University, Cambridge, Massachusetts 02138, USA

(Received 25 November 2012; revised manuscript received 16 February 2013; published 21 May 2013)

Origami structures are mechanical metamaterials with properties that arise almost exclusively from the geometry of the constituent folds and the constraint of piecewise isometric deformations. Here we characterize the geometry and planar and nonplanar effective elastic response of a simple periodically folded Miura-ori structure, which is composed of identical unit cells of mountain and valley folds with four-coordinated ridges, defined completely by two angles and two lengths. We show that the in-plane and out-of-plane Poisson's ratios are equal in magnitude, but opposite in sign, independent of material properties. Furthermore, we show that effective bending stiffness of the unit cell is singular, allowing us to characterize the two-dimensional deformation of a plate in terms of a one-dimensional theory. Finally, we solve the inverse design problem of determining the geometric parameters for the optimal geometric and mechanical response of these extreme structures.

DOI: 10.1103/PhysRevLett.110.215501 PACS numbers: 81.05.Xj, 46.70.De

Metamaterials are defined as materials whose structure and constitution allows them to have unusual emergent properties, such as negative refractive index optical metamaterials [1], or negative Poisson ratio mechanical metamaterials [2]. Here, we focus on origami-inspired mechanical metamaterials that arise as folded and pleated structures in a variety of natural systems including insect wings [3], leaves [4], and flower petals [5]. Using the presence of creases in these systems allows one to fold and unfold an entire structure simultaneously and design deployable structures such as solar sails [6] and foldable maps [7], and auxetic structural materials such as foams [8], and microporous polymers [9]. Indeed, folded sheets with reentrant geometries serve as models for crystal structures [10,11], molecular networks [12], and glasses [2] in a variety of physical applications. Complementing these studies, there has been a surge of interest in the mathematical properties of these folded structures [13–15], and some recent qualitative studies on the engineering aspects of origami [16–18]. In addition, the ability to create them *de novo* without a folding template, as a self-organized buckling pattern when a stiff skin resting on a soft foundation is subject to biaxial compression [19–21] has opened up a range of questions associated with their assembly in space and time, and their properties. However, most past quantitative work on these materials has been limited to understanding their behavior in two dimensions, either by considering their auxetic behavior in the plane, or the bending of a one-dimensional corrugated strip. In this Letter, we characterize the three-dimensional elastic response, Poisson's ratios, and rigidities of perhaps the simplest such mechanical metamaterial based on origami—a three-dimensional periodically pleated or folded structure, the Miura-ori pattern, [Fig. 1(a)] which is defined completely in terms of two angles and two lengths.

The geometry of the unit cell embodies the basic element in all nontrivial pleated structures—the mountain or valley fold, wherein four edges (folds) come together at a single vertex, as shown in Fig. 1(d). It is parametrized by two dihedral angles $\theta \in [0, \pi]$, $\beta \in [0, \pi]$, and one oblique angle α, in a cell of length l, width w, and height h. We treat the structure as being made of identical periodic rigid skew plaquettes joined by elastic hinges at the ridges. The structure can deploy uniformly in the plane [Fig. 1(b)] by having each constituent skew plaquette in a unit cell

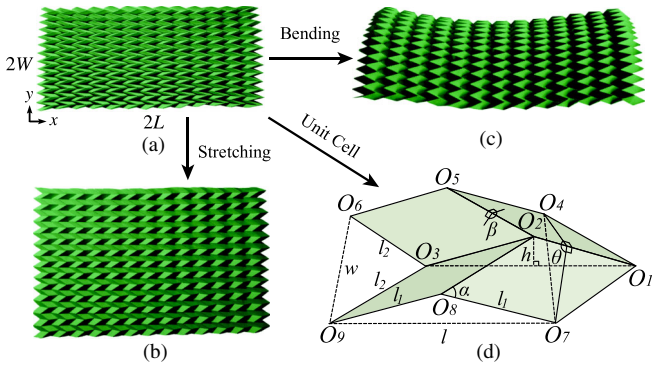

FIG. 1 (color online). Geometry of Miura-ori pattern. (a) A Miura-ori plate folded from a letter size paper contains 13 by 13 unit cells (along x and y directions, respectively), with $\alpha = 45°$ and $l_1 = l_2 = l_e$. The plate dimension is $2L$ by $2W$. (b) In-plane stretching behavior of a Miura-ori plate when pulled along the x direction shows it expands in all directions; i.e., it has a negative Poisson's ratio. (c) Out-of-plane bending behavior of a Miura-ori plate when a symmetric bending moment is applied on boundaries $x = \pm L$ shows a saddle shape, consistent with that, in this mode of deformation, its Poisson's ratio is positive. (d) Unit cell of Miura-ori is characterized by two angles α and θ given l_1 and l_2 and is symmetric about the central plane passing through $O_1O_2O_3$.

rotate rigidly about the connecting elastic ridges. Then the ridge lengths l_1, l_2, and $\alpha \in [0, \pi/2]$ are constant through folding or unfolding, so that we may choose θ (or equivalently β) to be the only degree of freedom that completely characterizes a Miura-ori cell. The geometry of the unit cell implies that

$$\beta = 2\sin^{-1}[\zeta \sin(\theta/2)], \qquad l = 2l_1\zeta, \\ w = 2l_2\xi \quad \text{and} \quad h = l_1\zeta \tan\alpha \cos(\theta/2), \tag{1}$$

where the dimensionless width and height are

$$\xi = \sin\alpha \sin(\theta/2) \quad \text{and} \quad \zeta = \cos\alpha(1 - \xi^2)^{-1/2}. \tag{2}$$

We see that β, l, w, and h change monotonically as $\theta \in [0, \pi]$, with $\beta \in [0, \pi]$, $l \in 2l_1[\cos\alpha, 1]$, $w \in 2l_2[0, \sin\alpha]$, and $h \in l_1[\sin\alpha, 0]$. As $\alpha \in [0, \pi/2]$, we see that $\beta \in [\theta, 0]$, $l \in [2l_1, 0]$, $w \in [0, 2l_2 \sin(\theta/2)]$, and $h \in [0, l_1]$. The geometry of the unit cell implies a number of interesting properties associated with the expansion kinematics of a folded Miura-ori sheet, including design optimization for packing, and the study of nearly orthogonal folds when $\alpha \approx \pi/2$, the singular case corresponding to the common map fold where the folds are all independent (SI-1 in Supplemental Material [22]). To minimize algebraic complexity and focus on the main consequences of isometric deformations of these structures, we will henceforth assume each plaquette is a rhombus, i.e., $l_1 = l_2 = l_e$.

The planar response of Miura-ori may be characterized in terms of two quantities—the Poisson's ratio which describes the coupling of deformations in orthogonal directions, and the stretching rigidity which characterizes its planar mechanical stiffness. The linearized planar Poisson's ratio is defined as

$$\nu_{wl} \equiv -\frac{dw/w}{dl/l} = 1 - \xi^{-2}. \tag{3}$$

It immediately follows that the reciprocal Poisson's ratio $\nu_{lw} = 1/\nu_{wl}$. Because $\xi \leq 1$, the in-plane Poisson's ratio $\nu_{wl} < 0$ [Fig. 2(a)]; i.e., Miura-ori is an auxetic material. The limits on ν_{wl} may be determined by considering the extreme values of α, θ, since ν_{wl} monotonically increases in both variables. Using the expression (2) in (3) and expanding the result shows that $\nu_{wl}|_{\alpha\to 0} \sim \alpha^{-2}$, and thus, $\nu_{wl}|_\theta \in (-\infty, -\cot^2(\theta/2)]$, while $\nu_{wl}|_{\theta\to 0} \sim \theta^{-2}$ and, thus, $\nu_{wl}|_\alpha \in (-\infty, -\cot^2\alpha]$. When $(\alpha, \theta) = (\pi/2, \pi)$, $\nu_{wl} = 0$ so that the two orthogonal planar directions may be folded or unfolded independently, as in traditional map folding. Indeed, this is the unique state for which nonparallel folds are independent, and it might surprise the reader that, with few exceptions, this is the way maps are folded—makes unfolding easy, but folding frustrating! The Poisson's ratios related to height changes, ν_{hl} and ν_{wh} can also be determined using similar arguments (SI-2.1 in Supplemental Material [22]).

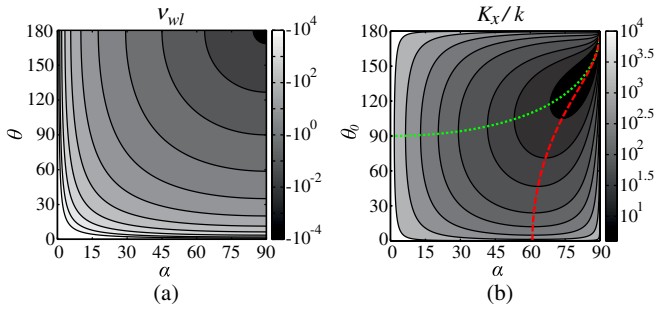

FIG. 2 (color online). In-plane stretching response of a unit cell. (a) Contour plot of Poisson's ratio ν_{wl}. ν_{wl} shows that it monotonically increases with both α and θ. $\nu_{wl}|_\alpha \in [-\infty, -\cot^2\alpha]$, and $\nu_{wl}|_\theta \in [-\infty, -\cot^2(\theta/2)]$. (b) Contour plot of the dimensionless stretching rigidity K_x/k. The green dotted curve indicates the optimal design angle pairs that correspond to the minima of $K_x|_\alpha$. The red dashed curve indicates the optimal design angle pairs that correspond to the minima of $K_x|_{\theta_0}$. See the text for details.

To calculate the in-plane stiffness of the unit cell, we note that the potential energy of a unit cell deformed by a uniaxial force f_x in the x direction is $H = U - \int_{\theta_0}^{\theta} f_x(dl/d\theta')d\theta'$, assuming that the elastic energy of a unit cell is stored only in the elastic hinges which allow the rigid plaquettes to rotate isometrically, with $U = kl_e(\theta - \theta_0)^2 + kl_e(\beta - \beta_0)^2$, k being the hinge spring constant, θ_0 and β_0 [$= \beta(\alpha, \theta_0)$] being the natural dihedral angles in the undeformed state. Then, the external force f_x at equilibrium is determined by the relation $\delta H/\delta\theta = 0$, while the stretching rigidity in the x direction is given by

$$K_x(\alpha, \theta_0) \equiv \frac{df_x}{d\theta}\bigg|_{\theta_0} = \frac{4k[(1 - \xi_0^2)^2 + \cos^2\alpha]}{(1 - \xi_0^2)^{1/2}\cos\alpha\sin^2\alpha\sin\theta_0}, \tag{4}$$

where $\xi_0 = \xi(\alpha, \theta_0)$ and ξ is defined in (2). To understand the bounds on K_x, we expand (4) in the vicinity of the extreme values of α and θ_0 which gives us $K_x|_{\alpha\to 0} \sim \alpha^{-2}$, $K_x|_{\alpha\to\pi/2} \sim (\pi/2 - \alpha)^{-1}$, $K_x|_{\theta_0\to 0} \sim \theta_0^{-1}$, and $K_x|_{\theta_0\to\pi} \sim (\pi - \theta_0)^{-1}$. As expected, we see that K_x has a singularity at $(\alpha, \theta_0) = (\pi/2, \pi)$, corresponding to the case of an almost flat, unfolded orthogonal Miura sheet.

We note that K_x is not a monotonic function of the geometric variables defining the unit cell, α and θ_0. Setting $\partial_{\theta_0} K_x|_\alpha = 0$ and $\partial_\alpha K_x|_{\theta_0} = 0$ allows us to determine the optimal design curves, $\theta_{0m}(\alpha)$ [green dotted curve in Fig. 2(b)] and $\alpha_m(\theta_0)$ [red dashed curve in Fig. 2(b)] that yield the minimum value of the stiffness K_x as a function of these parameters. Along these curves, the stiffness varies monotonically. Analogous arguments allow us to determine the orthogonal stretching rigidity K_y, which is related geometrically to K_x via the design angles α and θ (SI-2.2, 2.3 in Supplemental Material [22]). Since piecewise isometric deformations only allow for planar folding as the only possible motion using rigid

rhombus plaquettes in Miura-ori plates (SI-3.1 in Supplemental Material [22]), the in-plane shear elastic constant is infinite, an unusual result given that most normal materials may be sheared easily and yet strongly resist volumetric changes.

To understand the nonplanar bending response of Miura-ori, we must consider the conditions when it is possible to bend a unit cell isometrically, i.e., with only rotations of the plaquettes about their linking hinges. Minimally, isometric deformations require the introduction of one additional diagonal fold into each plaquette [Fig. 3(a)], either a short one (e.g., O_2O_7) or a long one (e.g., O_1O_8). Here, we adopt the short fold, as a result of which four additional degrees of freedom arise in each unit cell and allow for both symmetric bending and asymmetric twisting, depending on whether the rotations are symmetric or not. The out-of-plane bending Poisson's ratio $\nu_b \equiv -\kappa_y/\kappa_x$ [23], where κ_x, κ_y are the effective curvatures of the Miura-ori sheet in the x and y directions given by

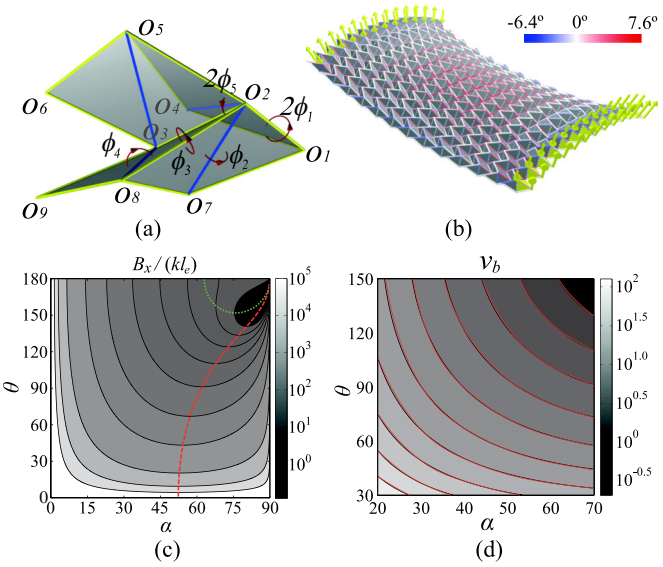

FIG. 3 (color online). Out-of-plane bending response of a unit cell. (a) The plaquettes deformations about each fold are symmetric about the plane $O_1O_2O_3$, so that the angles $2\phi_1$, ϕ_2, ϕ_3, ϕ_4, and $2\phi_5$ correspond to rotations about the axes $\overrightarrow{O_1O_2}$, $\overrightarrow{O_7O_2}$, $\overrightarrow{O_2O_8}$, $\overrightarrow{O_8O_3}$, and $\overrightarrow{O_3O_2}$, respectively. (b) Numerical simulation of the bending of a Miura-ori plate with $\alpha = 45°$ and $\theta = 90°$. Force dipoles are shown by yellow arrows. Color of the folds indicates the value of deformation angles. (c) Contour plot of dimensionless bending stiffness $B_x/(kl_e)$ corresponding to pure bending of a unit cell. The green dotted curve and red dashed curve indicate the optimal design angle pairs that correspond to the local minima of $B_x|_\alpha$ and $B_x|_\theta$, respectively. (d) Contour plot of bending Poisson's ratio. The gray scale plot is from the analytic expression (6) and the red curves are extracted from simulation results. In our simulations, we use a plate made of 21 by 21 unit cells and vary α from 20° to 70°, θ from 30° to 150° both every 10°.

$$\kappa_x = \frac{\cos(\alpha/2)\sin(\theta/2)}{2l_e\sqrt{1-\xi^2}}(\phi_2+\phi_4),$$
$$\kappa_y = -\frac{\sqrt{1-\xi^2}}{4l_e\sin(\alpha/2)\xi}(\phi_2+\phi_4), \tag{5}$$

with κ_x being the dihedral angle between plane $O_6O_3O_9$ and $O_4O_1O_7$ [Fig. 3(a)] projected onto the x direction over the unit cell length (SI-3.2 in Supplemental Material [22]), and κ_y being the dihedral angle between plane $O_4O_5O_6$ and $O_7O_8O_9$ projected onto the y direction over the unit cell width. The angles ϕ_2, ϕ_4 characterize rotations about internal folds $\overrightarrow{O_7O_2}$ and $\overrightarrow{O_8O_3}$, respectively, and are deemed positive according to the right-hand rule. We note that although there are a total of five deformation angles [Fig. 3(a)], both κ_x and κ_y depend only on ϕ_2 and ϕ_4. This is because of the symmetry of deformations about the xoz plane; ϕ_3 and ϕ_5 are functions of ϕ_1 and ϕ_2 (Eq. S.28 in Supplemental Material [22]), and the case that ϕ_1 changes, while keeping ϕ_2 and ϕ_4 zero, corresponds to the planar stretch of a unit cell, so ϕ_1 does not contribute to both curvatures. This is consistent with our intuition that bending a unit cell requires the bending of plaquettes. The Poisson's ratio for bending, thus, is

$$\nu_b = -\frac{\kappa_y}{\kappa_x} = -1 + \xi^{-2} = -\nu_{wl}, \tag{6}$$

where the last equality follows from Eqs. (3) and (5). If the original plaquettes are allowed to fold along the long diagonals instead [e.g., O_8O_1 in Fig. 3(a)], the new curvature components κ_x and κ_y are still given by (5) with α being replaced by $\pi - \alpha$ (SI-3.3 in Supplemental Material [22]), and ϕ_2, ϕ_4 now being rotations about axis $\overrightarrow{O_8O_1}$ and $\overrightarrow{O_9O_2}$, respectively. Therefore, $\nu_b = -\kappa_y/\kappa_x = -\nu_{wl}$. We note that in nonplanar bending, the sheet behaves like a normal material, deforming into a saddle as shown in Fig. 1(c). The surprising result, that the in-plane Poisson's ratio is equal in magnitude but opposite in sign to the out-of-plane Poisson ratio, is independent of the mechanical properties of the sheet and is a consequence of geometry alone. Although our analysis is limited to the case when the deformation involves only small changes in the angles about their natural values, this is not as restrictive as it seems, since small changes to the unit cell can still lead to very large global deformations of the entire sheet.

Given our understanding of the geometry of bending in a unit cell, we now derive an effective continuum elastic theory for a Miura-ori plate that consists of many unit cells. Our calculations for the unit cell embodied in (5) show that κ_x/κ_y is only a function of the design angles α and θ, and independent of deformation angles; i.e., one cannot independently control κ_x and κ_y. Physically, this means that purely cylindrical deformations with zero

Gaussian curvature are impossible, as locally the unit cell can only be bent into a saddle with negative Gaussian curvature. In the continuum limit, this implies that the effective stiffness matrix [24] of a two-dimensional Miura-ori plate is singular, and has rank one. Thus, the two-dimensional deformations of a Miura plate can be described completely by a one-dimensional beam theory.

To calculate the bending stiffness per unit width of a single cell in the x direction B_x, we note that the elastic energy is physically stored in the eight discrete folds [Fig. 3(a)] and thus, is expressed as $kl_e(2\phi_1^2+\phi_3^2+2\phi_5^2)+2k_pl_e\sin(\alpha/2)(\phi_4^2+\phi_2^2)$, where k and k_p are the spring constants of the ridges and the diagonal folds of plaquettes, respectively. In an effective continuum theory, the energy associated with the deformations of the unit cell when bent into a sheet may be described in terms of its curvatures. Thus, associated with the curvature κ_x, the energy per unit area of the sheet is $(1/2)B_xwl\kappa_x^2$, where the effective bending stiffness B_x is derived by equating the discrete and continuous versions of the energy and inserting w, l from (1) and κ_x from (5). In general, B_x depends on multiple independent deformation angles, but we start by studying the "pure bending" case, where a row of unit cells aligned in the x direction undergo the same deformation and stretching is constrained, i.e., $\phi_1 = 0$ for all cells so that $\phi_2 = \phi_4$. In this well-defined limit, $\phi_3 = (1/2)\phi_2\csc(\alpha/2)[1-2\cos\alpha/(1-\xi^2)]$ and $\phi_5 = (1/2)\phi_2\csc(\alpha/2)$, so that

$$B_x(\alpha,\theta) = kl_e\left[2+16\frac{k_p}{k}\sin^3\frac{\alpha}{2}+\left(1-\frac{2\cos\alpha}{1-\xi^2}\right)^2\right] \times\cot\left(\frac{\theta}{2}\right)\frac{(1-\xi^2)^{3/2}}{2\xi^2\cos\alpha\sin\alpha\cos(\theta/2)}. \quad (7)$$

The bending stiffness per unit width of a single cell in the y direction B_y is related to B_x via the expression for bending Poisson's ratio $\nu_b^2 = B_x/B_y$, where ν_b is defined in (6). Just as there are optimum design parameters that allow us to extremize the in-plane rigidities, we can also find the optimal design angle pairs that minimize B_x, by setting $\partial_\theta B_x|_\alpha = 0$ and $\partial_\alpha B_x|_\theta = 0$. This gives us two curves $\theta_m(\alpha)$ and $\alpha_m(\theta)$ shown in Fig. 3(c), where we have assumed $k = k_p$. To understand the bounds on B_x, we expand (7) in the vicinity of the extreme values of the design variables α and θ and find that $B_x|_{\alpha\to 0}\sim\alpha^{-3}$, $B_x|_{\alpha\to\pi/2}\sim(\pi/2-\alpha)^{-1}$, and $B_x|_{\theta\to 0}\sim\theta^{-3}$. We see that $B_x|_{\theta\to\pi}$ is bounded except when $(\alpha,\theta)=(\pi/2,\pi)$, corresponding to the case of an almost flat, unfolded orthogonal Miura sheet. Given the geometric relation between B_x and B_y, we note that optimizing B_y is tantamount to extremizing B_x.

The deformation response of a complete Miura-ori plate requires a numerical approach because it is impossible to assemble an entire bent plate by periodically aligning unit cells with identical bending deformations in both the x and y directions. Our numerical model takes the form of a simple triangular-element based discretization of the sheet, in which each edge is treated as a linear spring with stiffness inversely proportional to its rest length. Each pair of adjacent triangles is assigned an elastic hinge with a bending energy quadratic in its deviation from an initial rest angle that is chosen to reflect the natural shape of the Miura-ori plate. We compute the elastic stretching forces and bending torques in a deformed mesh [25,26], assigning a scaled stretching stiffness that is six orders of magnitude larger than the bending stiffness of the adjacent facets, so that we may deform the mesh nearly isometrically. When our numerical model of a Miura-ori plate is bent by applied force dipoles along its left-right boundaries, it deforms into a saddle [Fig. 3(b)]. In this state, asymmetric inhomogeneous twisting arises in most unit cells; indeed this is the reason for the failure of averaging for this problem, since different unit cells deform differently, and we cannot derive an effective theory by considering just the unit cell. This is in contrast with the in-plane case, where the deformations of the unit cell are affinely related to those of the entire plate. Our results also show that the maximal stresses typically arise in the middle of the Miura-ori plate, away from boundaries. Thus, in a real plate, the vertices and hinges near the center are likely to fail first unless they are reinforced.

We now compare our predictions for the bending Poisson's ratio ν_b of the one-dimensional beam theory with those determined using full two-dimensional simulations. In Fig. 3(d), we plot ν_b from (6) (the gray scale contour plot) based on a unit cell and ν_b extracted at the center of the bent Miura-ori plate from simulations (the red curves). In the center of the plate where only symmetric bending and in-plane stretching modes are activated, the two approaches agree, but away from the center where this symmetry is violated, this is no longer true.

Folded structures, mechanical metamaterials might be named Orikozo, from the Japanese for folded matter. Our analysis of the simplest of these structures is rooted in the geometry of the unit cell as characterized by a pair of design angles α and θ together with the constraint of piecewise isometric deformations. We have found simple expressions for the linearized planar stretching rigidities K_x, K_y, and nonplanar bending rigidities B_x and B_y, and shown that the bending response of a plate can be described in terms of that of a one-dimensional beam. Furthermore, we find that the in-plane Poisson's ratio $\nu_{wl} < 0$, while the out-of-plane bending Poisson ration $\nu_b > 0$, an unusual combination that is not seen in simple materials, satisfying the general relation $\nu_{wl} = -\nu_l$, a consequence of geometry alone. Our analysis also allows us to pose and solve a series of design problems to find the optimal geometric parameters of the unit cell that lead to extrema of stretching and bending rigidities as well as contraction or expansion ratios of the system. This paves the way for the use of optimally designed Miura-ori patterns in three-dimensional nanostructure fabrication [27], and raises

the possibility of optimal control of actuated origami-based materials in soft robotics [28] and elsewhere using the simple geometrical mechanics approaches introduced here.

We thank the Wood lab for help with laser cutting the Miura-ori plates, the Wyss Institute and the Kavli Institute for support, and Tadashi Tokieda for discussions and the nomenclature Orikozo for these materials.

Note added in proof.—While our paper was under review, an experimental engineering study on foldable structures was published [29] consistent with our comprehensive theoretical and computational approach to the geometry and mechanics of Miura-ori.

*lm@seas.harvard.edu

[1] D. R. Smith, J. B. Pendry, and M. C. Wiltshire, Science **305**, 788 (2004).
[2] G. N. Greaves, A. L. Greer, R. S. Lakes, and T. Rouxel, Nat. Mater. **10**, 823 (2011).
[3] Wm. T. M. Forbes, Psyche **31**, 254 (1924).
[4] H. Kobayashi, B. Kresling, and J. F. V. Vincent, Proc. R. Soc. B **265**, 147 (1998).
[5] H. Kobayashi, M. Daimaruya, and H. Fujita, Solid Mech. Its Appl. **106**, 207 (2003).
[6] K. Miura, in *Proceedings of 31st Congress International Astronautical Federation, Tokyo*, 1980, IAF-80-A 31:1-10.
[7] E. A. Elsayed and B. B. Basily, Int. J. Mater. Prod. Technol. **21**, 217 (2004).
[8] R. S. Lakes, Science **235**, 1038 (1987).
[9] B. D. Caddock and K. E. Evans, J. Phys. D **22**, 1877 (1989); K. E. Evans and B. D. Caddock, J. Phys. D **22**, 1883 (1989).
[10] A. Y. Haeri, D. J. Weidner, and J. B. Parise, Science **257**, 650 (1992).
[11] A. L. Goodwin, D. A. Keen, and G. Tucker, Proc. Natl. Acad. Sci. U.S.A. **105**, 18 708 (2008).
[12] K. E. Evans, M. A. Nkansah, J. Hutchinson, and S. C. Rogers, Nature (London) **353**, 124 (1991).
[13] R. Lang, *Origami Design Secrets: Mathematical Methods for an Ancient Art* (A K Peters/CRC Press, Boca Raton, FL, 2011), 2nd ed.
[14] E. Demaine and J. O'Rourke, *Geometric Folding Algorithms: Linkages, Origami, Polyhedra* (Cambridge University Press, Cambridge, England, 2007).
[15] T. Hull, *Project Origami: Activities for Exploring Mathematics* (A K Peters/CRC Press, Boca Raton, FL, 2011).
[16] Y. Klettand and K. Drechsler, in *Origami5: International Meeting of Origami, Science, Mathematics, and Education*, edited by P. Wang-Iverson, R. J. Lang, and M. Yim (CRC Press, Boca Raton, FL, 2011), pp. 305–322.
[17] M. Schenk and S. Guest, in *Origami5: International Meeting of Origami, Science, Mathematics, and Education*, edited by P. Wang-Iverson, R. J. Lang, and M. Yim (CRC Press, Boca Raton, FL, 2011), pp. 291–304.
[18] A. Papa and S. Pellegrino, J. Spacecr. Rockets **45**, 10 (2008).
[19] N. Bowden, S. Brittain, A. G. Evans, J. W. Hutchinson, and G. M. Whitesides, Nature (London) **393**, 146 (1998).
[20] L. Mahadevan and S. Rica, Science **307**, 1740 (2005).
[21] B. Audoly and A. Boudaoud, J. Mech. Phys. Solids **56**, 2444 (2008).
[22] See Supplemental Material at http://link.aps.org/supplemental/10.1103/PhysRevLett.110.215501 for detailed derivations.
[23] In general, the incremental Poisson's ratio is $\nu_b = -d\kappa_y/d\kappa_x$, but here, we only consider linear deformations about the flat state, so $\nu_b = -\kappa_y/\kappa_x$.
[24] E. Ventsel and T. Krauthammer, *Thin Plates and Shells: Theory, Analysis, and Applications* (CRC Press, Boca Raton, FL, 2001), 1st ed., pp. 197–199.
[25] R. Bridson, S. Marino, and R. Fedkiw, ACM SIGGRAPH/Eurograph. Symp. Comp. Animation (SCA) (2003), pp. 28–36.
[26] R. Burgoon, E. Grinspun, and Z. Wood, in *Proceedings of the ISCA 21st International Conference on Computers and Their Applications*, (ISCA, 2006), p. 180.
[27] W. J. Arora, A. J. Nichol, H. I. Smith, and G. Barbastathis, Appl. Phys. Lett. **88**, 053108 (2006).
[28] E. Hawkes, B. An, N. Benbernou, H. Tanaka, S. Kim, E. D. Demaine, D. Rus, and R. J. Wood, Proc. Natl. Acad. Sci. U.S.A. **107**, 12 441 (2010).
[29] M. Schenk and S. Guest, Proc. Natl. Acad. Sci. U.S.A. **110**, 3276 (2013).